THE JOURNAL OF PHYSICAL CHEMISTRY B

Article

pubs.acs.org/JPCB

Melting–Freezing Transition of Monolayer Water Confined by Phosphorene Plates

G. X. Nie,[†,‡] J. Y. Huang,*[,†,‡] and J. P. Huang*[,†,‡]

[†]Department of Physics and State Key Laboratory of Surface Physics, Fudan University, Shanghai 200433, China

[‡]Collaborative Innovation Center of Advanced Microstructures, Nanjing 210093, China

ABSTRACT: The two-dimensional material phosphorene has become a focus of the scientific community recently. On the basis of molecular dynamics simulations, we utilize phosphorene as a model material to study the behavior of water molecules confined by two phosphorene plates with nonflat surfaces. As the relative position of the two plates changes, the water molecules first stay in a melting process at 230 K and then exhibit a freezing process. The disparate variations of local confinements induced by the mismatch of the two plates are the key for understanding this extraordinary behavior of water. Our results imply that such nonflat surfaces could be an important factor for understanding or controlling the dynamics of water. The phenomena reported here may enrich the knowledge of water and inspire more applications of similar materials.

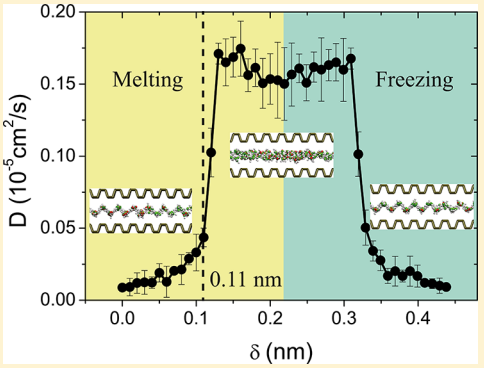

1. INTRODUCTION

The studies on confined water at the nanoscale have important implications in academics and in applications such as water transport across cell membranes,[1−7] water purification,[8−10] surface lubrication,[11,12] and protein folding.[13−16] Compared to bulk water, confined water exhibits novel behaviors. For example, the anomalous properties of water shift to lower temperatures in confined systems by ≈40 K relative to that in the bulk.[17] The behaviors of confined water are related to its temperature and pressure.[18] Also, they are expected to be affected notably by other conditions, such as the distance between two confining plates,[19,20] the hydrophilic–hydrophobic properties of the confining plates,[21,22] and the strength of external electric fields.[23−27] With molecular dynamics (MD) simulations, Koga et al.[28] proposed a phase diagram of confined water in the temperature–pressure–distance space. Kumar et al.[17] found that different crystalline structures form for two different distances of the plates, which were not observed in the bulk system. Zangi et al.[19] reported that the arrangement and mobility of water molecules are sensitive to the distance between two confining plates and a monolayer ice structure can form under extreme confinement at 300 K. Such a monolayer ice structure was later experimentally detected on aluminum oxide[30] and smooth SiO_2[31] surfaces. Giovambattista et al.[20] verified that water could form an ordered structure only when the distances between the plates and water density are appropriate. Furthermore, upon applying external electric fields, the molecular water thin films will undergo either an electrofreezing[23,24,26] or electromelting process.[25,27]

In practice, two-dimensional (2D) materials are often used as model confining plates to study the behaviors of confined water.[29] Since the recent synthesis of few-layered black phosphorus,[32−34] named phosphorene, the 2D phosphorous material has become a focus of the scientific community.[35−45] Phosphorene possesses a finite direct band gap and very high carrier mobility.[32] Field-effect transistors[32,43] and high-frequency nanoelectromechanical resonators[46] based on phosphorene have been reported. Owing to the puckered structure, this new material exhibits strongly anisotropic electronic, optical, and thermal properties,[36,38,41] which are disparate from those of other 2D materials investigated so far. Moreover, phosphorene has shown promising application prospects in biology, and the research on interfacial water on phosphorene surfaces is just beginning. On the basis of MD simulations, Zhang et al.[47] studied behaviors of water on pristine and strained phosphorene surfaces. They found anisotropic diffusion of water and different water structures when phosphorene is stretched transversely and longitudinally. Compared to the flat surface of usual confining plates,[23−27] the nonflat surface of phosphorene may give rise to new insights into behaviors of confined water. However, how such nonflat surface affects the behavior of confined water has rarely been discussed.

In this work, slit phosphorene pores are used as a model system to explore the behaviors of monolayer water confined by nonflat materials. Through MD simulations, a melting–freezing transition of monolayer water is observed when the relative position of the two confining plates changes. The disparate variations of local confinements induced by the mismatch of two confining plates are the key for understanding this extraordinary behavior of water.

Received: March 9, 2016
Revised: July 30, 2016
Published: August 1, 2016

DOI: 10.1021/acs.jpcb.6b02473
J. Phys. Chem. B 2016, 120, 9011−9018

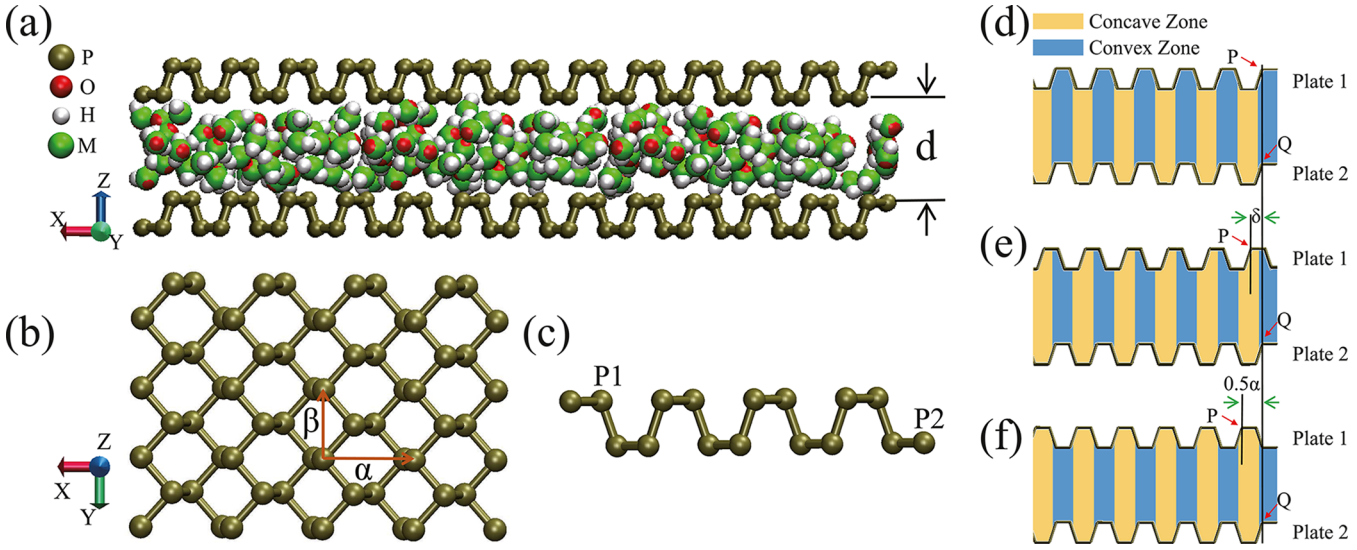

Figure 1. (a) Snapshot of our simulation system with 472 TIP4P water molecules confined between two parallel phosphorene plates within the *XY* plane. The distance between inner surfaces is denoted *d*, and *d* = 0.79 nm throughout this work; the four different atoms, P (phosphorus), O (oxygen), H (hydrogen), and M (dummy atom with negative charge), are indicated. (b)−(c) Top and side views of the structure of phosphorene, respectively, where the unit cell dimensions are (β, α) = (0.332, 0.438) nm. More details can be found in the article. (d)−(f) Sketch maps of the mismatch between plates 1 and 2. Atoms P and Q are used as references. Plate 2 (lower plate) is kept stationary. Plate 1 (upper plate) is moved along the *X* axis, and the distance between plates 1 and 2 along the *X* direction is denoted δ. Each δ corresponds to one simulation system. We define δ = 0 nm when the convexities of plates 1 and 2 are directly facing each other (d). Thus, $\delta = 0.5\alpha$ (0.219 nm) when the convexity of plate 2 is directly facing the concavity of plate 1 (f). For further discussion, the concave and convex zones are also indicated, and these are the spaces that the concavity and convexity of plate 2 face, respectively.

2. METHODS

We adopt MD simulations, which have been widely utilized for the study of water dynamics. Figure 1a displays our simulation framework containing 472 TIP4P[27,48−50] water molecules between two parallel phosphorene plates within the *XY* plane. The distance, *d*, between the inner surfaces of plates is 0.79 nm, which just accommodates one layer of water molecules. Phosphorene's structure is referred to ref 45. Figure 1b,c presents the top and side views of the phosphorene plate used in our study, respectively. The unit cell dimensions are (β, α) = (0.332, 0.438) nm. There are two sublayers in one phosphorene plate. Atoms in one sublayer are denoted P1, and atoms in the other sublayer are denoted P2, as shown in Figure 1c. The bond length of P1−P1 or P2−P2 is 0.223 nm, and the bond length of P1−P2 is 0.225 nm.

Previous works[25,27] achieved electromelting at 300 and 240 K for water molecules. In this work, we choose a canonical ensemble (the results of usually used NVT and NPT ensembles are the same; here, for investigating the effect of mismatch, the volume is fixed and the NVT ensemble is chosen.) at a lower temperature of 230 K by resorting to the MD package, Gromacs 4.0.7.[51] The van der Waals interactions between atoms are treated by the Lennard-Jones (LJ) potential, $V_{LJ} = 4\varepsilon\left[\left(\frac{\sigma}{r}\right)^{12} - \left(\frac{\sigma}{r}\right)^{6}\right]$, where ε is the depth of the potential well, σ is the finite distance at which the interatom potential is zero, and r is the distance between the atoms. The LJ interaction parameters of phosphorus atoms are ε_{PP} = 1.6736 kJ/mol and σ_{PP} = 0.333 nm.[45] Given that ε_{OO} = 0.6362 kJ/mol and σ_{OO} = 0.3150 nm and according to the Lorentz−Berthelot rules, water−plates interactions can be represented by LJ parameters ε_{OP} = 1.0319 kJ/mol and σ_{OP} = 0.32401 nm. The particle mesh Ewald method[52] is used for electrostatic interaction; evaluation of nonbonded interactions is performed using a twin-range cutoff of 1.0 and 1.5 nm for Coulombic and LJ potentials, respectively. We also adopt the thermostat of Nosé and Hoover[53,54] with a time constant of 0.5 ps. Besides, the leapfrog integration algorithm is used, and periodic boundaries are set in the simulation box with dimensions L_X, L_Y, L_Z, where L_X = 5.693 nm and L_Y = 5.970 nm. To avoid nonphysical results, we set L_Z = 30 nm, which is about 5 times of L_X or L_Y.[55]

We change the relative position of the two phosphorene plates along the *X* direction, making them mismatched. The upper plate (plate 1) is moved along the *X* direction, whereas the lower one (plate 2) is kept stationary (see Figure 1d−f). δ denotes the relative distance between plates 1 and 2 along the *X* direction, and each δ corresponds to one simulation system. For instance, in Figure 1d, the convexities of plates 1 and 2 are directly facing each other, which corresponds to the system of δ = 0 nm. When δ increases to be 0.5α (0.219 nm), the convexity of plate 2 is directly facing the concavity of plate 1, as shown in Figure 1f. When $\delta = \alpha$ (0.438 nm), the system is the same as that when δ = 0 nm. In each simulation, to make δ fixed and investigate the sole effect of mismatch between the nonflat plates on the behavior of water, phosphorene plates are set to be stationary. In our study, δ is increased from 0 nm to α by 0.01 nm, except when $\delta = 0.5\alpha$ (0.219 nm) and α (0.438 nm). The simulation for each δ set runs for 15 ns, with a time step of 2 fs, and the data from the last 10 ns are collected for analysis (we divide the last 10 ns into five intervals to get the error bars of each data). We consider that a hydrogen bond is formed between two water molecules when the O···O distance is shorter than 0.35 nm and simultaneously the O−H···O angle is less than 30°.

DOI: 10.1021/acs.jpcb.6b02473
J. Phys. Chem. B 2016, 120, 9011−9018

3. RESULTS

The lateral diffusion coefficients within the XY plane (D's) of water with respect to δ are calculated according to the Einstein relation, $D = \frac{1}{4t}\lim_{t\to\infty}\langle (x_i(t) - x_i(0))^2 + (y_i(t) - y_i(0))^2\rangle$, to measure water mobilities, and the results are shown in Figure 2a. When δ = 0 nm, a puckered monolayer ice structure

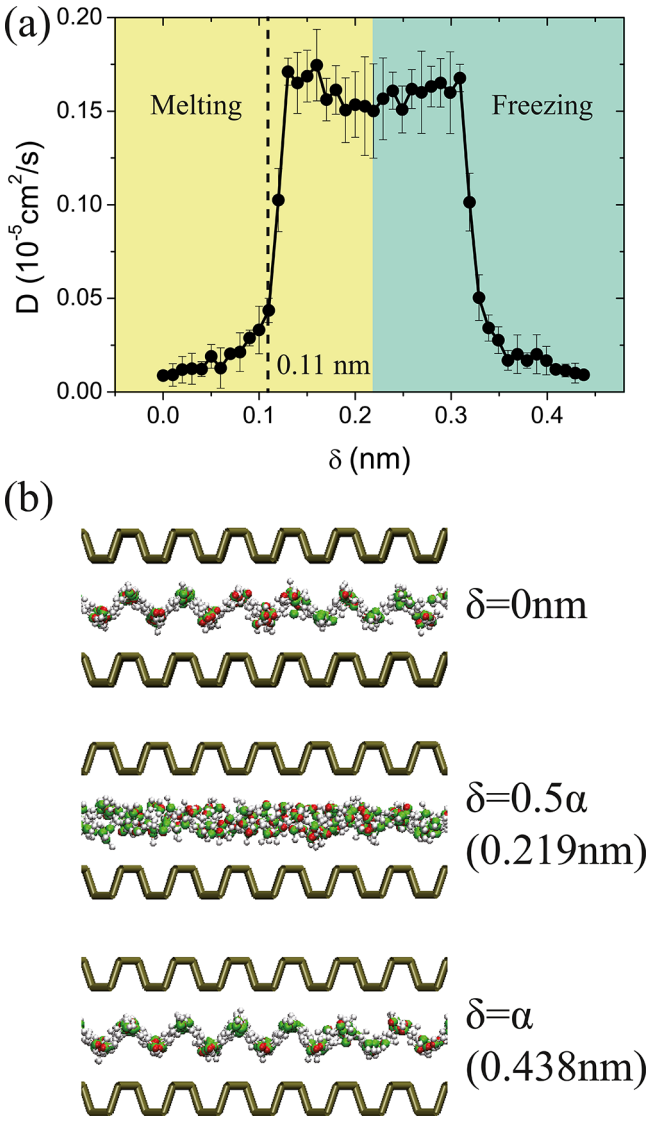

Figure 2. (a) Profile of the lateral diffusion coefficient of water molecules within the XY plane, D, with respect to δ. The evolution of D indicates that a melting process occurs when δ varies from 0 nm to 0.5α (0.219 nm) and a freezing process, as δ increases from 0.5α to α (0.438 nm). Typically, when δ = 0.11 nm (dashed line), D begins to increase sharply. δ is increased from 0 nm to α by 0.01 nm, except when $\delta = 0.5\alpha$ (0.219 nm) and α (0.438 nm). (b) Snapshots of the systems when δ = 0, 0.219, 0.438 nm.

forms (see Figure 2b). Such a puckered ice structure matches well with the puckered structure of phosphorene plates. The mobility of ice remains nearly unchanged for $\delta \leq 0.04$ nm, with lateral diffusion coefficients fluctuating slightly on the order of 10^{-8} cm^2 s^{-1}. When δ ranges from 0.04 to 0.1 nm, D increases gradually. Then, it sharply increases when δ = 0.11 nm (about 0.25α) and reaches the order of 10^{-6} cm^2 s^{-1} when δ = 0.12 nm (about 0.27α). After that, D fluctuates around 1.6×10^{-6} cm^2 s^{-1} (which is comparable to the lateral diffusion coefficients of ref 27 and the bulk water at 230 K, 3.788×10^{-6} cm^2 s^{-1}) when 0.13 nm $\leq \delta \leq 0.5\alpha$. At $\delta = 0.5\alpha$, it is found that water networks are disrupted (see Figure 2b), which greatly increases the mobility of water. These indicate that the monolayer water performs a melting process when δ is increased from 0 nm to 0.5α (the Lindemann criterion could also be a suitable justification for the melting process[21]). With increasing δ, D drops suddenly and water molecules arrange in an orderly manner again (see Figure 2b), implying a freezing process. In general, as δ varies from 0 nm to α, we observe a melting process and a freezing process, which are symmetric with respect to $\delta = 0.5\alpha$. Since the variation of configurations of confining plates caused by δ is also symmetric with respect to $\delta = 0.5\alpha$, freezing is an inverse process of melting. Thus, in the following discussions, only the melting process (i.e., 0 nm $\leq \delta \leq 0.5\alpha$) is considered. The effect of global confinement (Section 4.1) and local confinement (Section 4.2) on the system and the hydrogen bonding (Section 4.3) are discussed.

4. DISCUSSION

4.1. Effect of Global Confinement. Due to the puckered structure of phosphorene, as δ increases from 0 nm to 0.5α, the interaction between water and plates changes. The average interaction energy between each water molecule and plates with respect to δ is calculated with LJ potentials, and it is plotted in Figure 3a. With an increase in δ, the interaction energy increases, which implies that the global confinement caused by plates strengthens. Thus, water molecules are squeezed further away from the surfaces of the plates. Figure 3b shows the density distributions of water along the Z direction, and the positions of oxygen atoms represent the mass centers of water molecules. The value of the horizontal ordinate (Z) is the distance from the inner surface of plate 2. Z = 0.395 nm is the middle plane of the system. When water is solid, the arrangement of water molecules is ordered and the density distribution of water is more concentrated. Thus, the peaks in Figure 3b are higher and thinner. With an increase in δ, the peaks get lower and wider. Under such an enhancing global confinement, water is squeezed and its solid characteristic diminishes. Regarding the pressure, we have calculated the lateral pressure of water within the XY plane, P_{XY} (see Figure 3c). P_{XY} fluctuates around 3.2 bar for δ = 0−0.04 nm, and then it increases to be around 4.6 bar for δ = 0.12−0.219 nm. The perpendicular pressure, P_Z, is much greater (about 26 000 times) than P_{XY} (see Figure 3d). This is attributed to the strong confinement effect of the nanosystem. Also, P_Z increases with an increase in δ. Figure 3e plots the density of water in the system, ρ_t, as a function of δ. As δ increases, ρ_t fluctuates around 0.84 g/cm^3.

4.2. Effect of Local Confinement. When δ = 0 nm, the puckered monolayer ice structure matches well with that of the confined space (see Figure 2b). However, as δ increases, the confining plates become mismatched and ice networks get disrupted. To clarify what happened to water molecules when plates are mismatched, two types of zones, concave and convex zones, are defined accordingly. The concave and convex zones correspond to the space with the concavity and convexity of plate 2 (see Figure 1d−f). The boundaries between the two zones are located at the middle points of bonds P1−P2 of plate 2 (see Figure 1c−f). When δ = 0 nm, the volumes of the two zones are equal. As plates become mismatched, the atoms in the lower sublayer of plate 1 move into the convex zone. Thus,

DOI: 10.1021/acs.jpcb.6b02473
J. Phys. Chem. B 2016, 120, 9011−9018

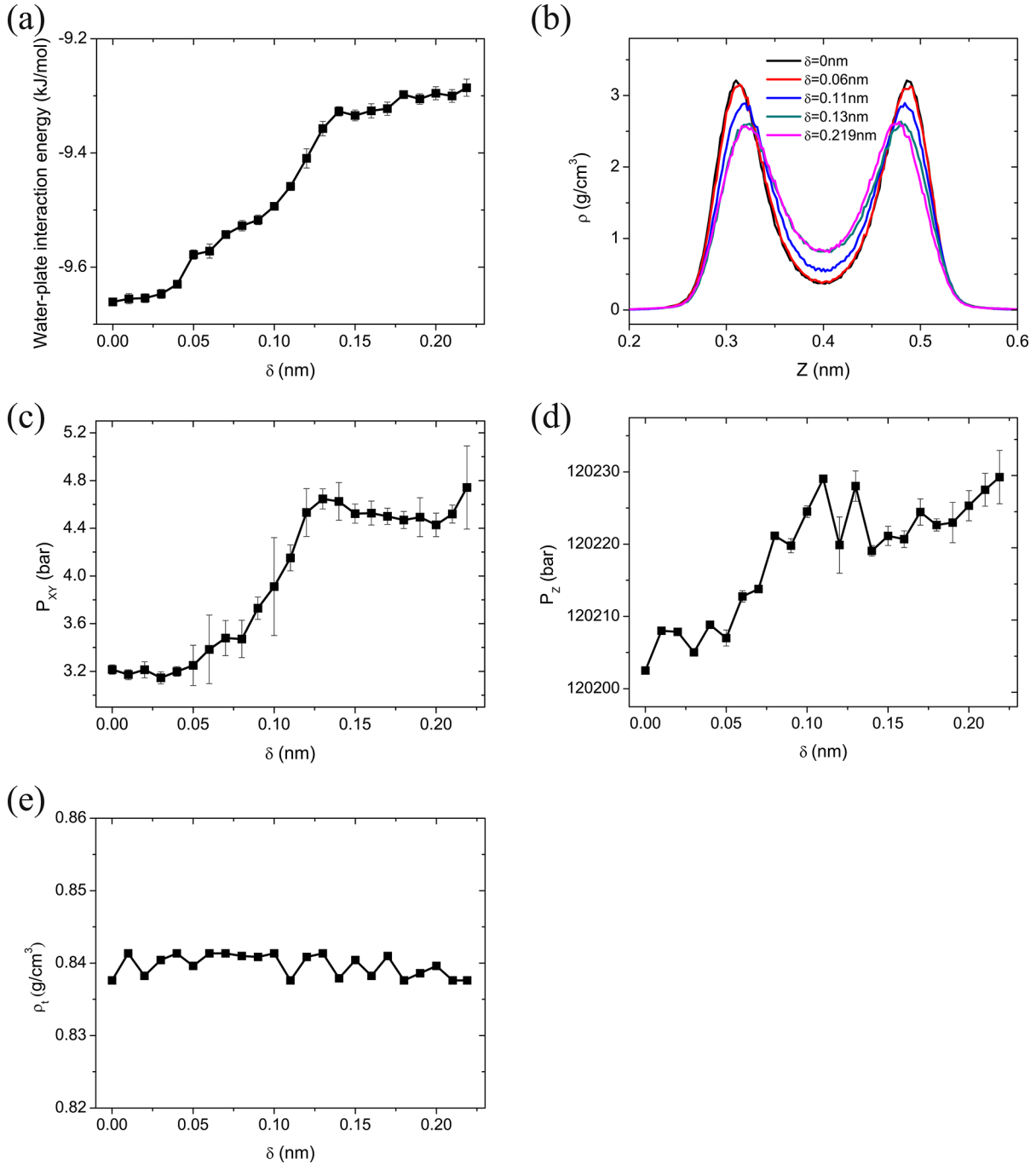

Figure 3. (a) Average water−plate interaction energies with respect to δ. The interaction energy increases as δ increases. (b) Density distribution of water along the Z axis in systems with δ = 0, 0.06, 0.11, 0.13, and 0.219 nm. The positions of oxygen atoms represent the mass centers of water molecules. The value of the horizontal ordinate (Z) is the distance from the inner surface of plate 2. As δ increases, two oxygen planes get closer and the peaks drop. (c) Lateral pressure within the XY plane, P_{XY}, with respect to δ. (d) Perpendicular pressure, P_Z, with respect to δ. (e) Density of water in the system, ρ_t, with respect to δ.

the convex zone shrinks, whereas the concave zone expands. Although the distance between the inner surfaces of plates, d, is kept to be 0.79 nm, the local confinement changes. Figure 4a displays the average water−plate interaction energies in the concave and convex zones, and the positions of oxygen atoms represent the mass centers of water molecules. The negative values of energies indicate attraction between water and plates. With increasing δ, the interaction energies between the plates and water molecules in both zones strengthen first and then fluctuate within a small range. However, the interaction energy in the convex zone grows faster than that in the concave zone, and their difference starts to increase extensively when δ = 0.11 nm. This manifests that the variations of local confinements in the two zones are different. Figure 4b exhibits the average water−water interaction energy, and its negative value indicates attraction between water molecules. The water−water interaction energy decreases gradually in the concave zone as δ increases, indicating strengthening attraction between water molecules. In the convex zone, the energy increases gradually first and then sharply at δ = 0.11 nm, which indicates a weaker

DOI: 10.1021/acs.jpcb.6b02473
J. Phys. Chem. B 2016, 120, 9011−9018

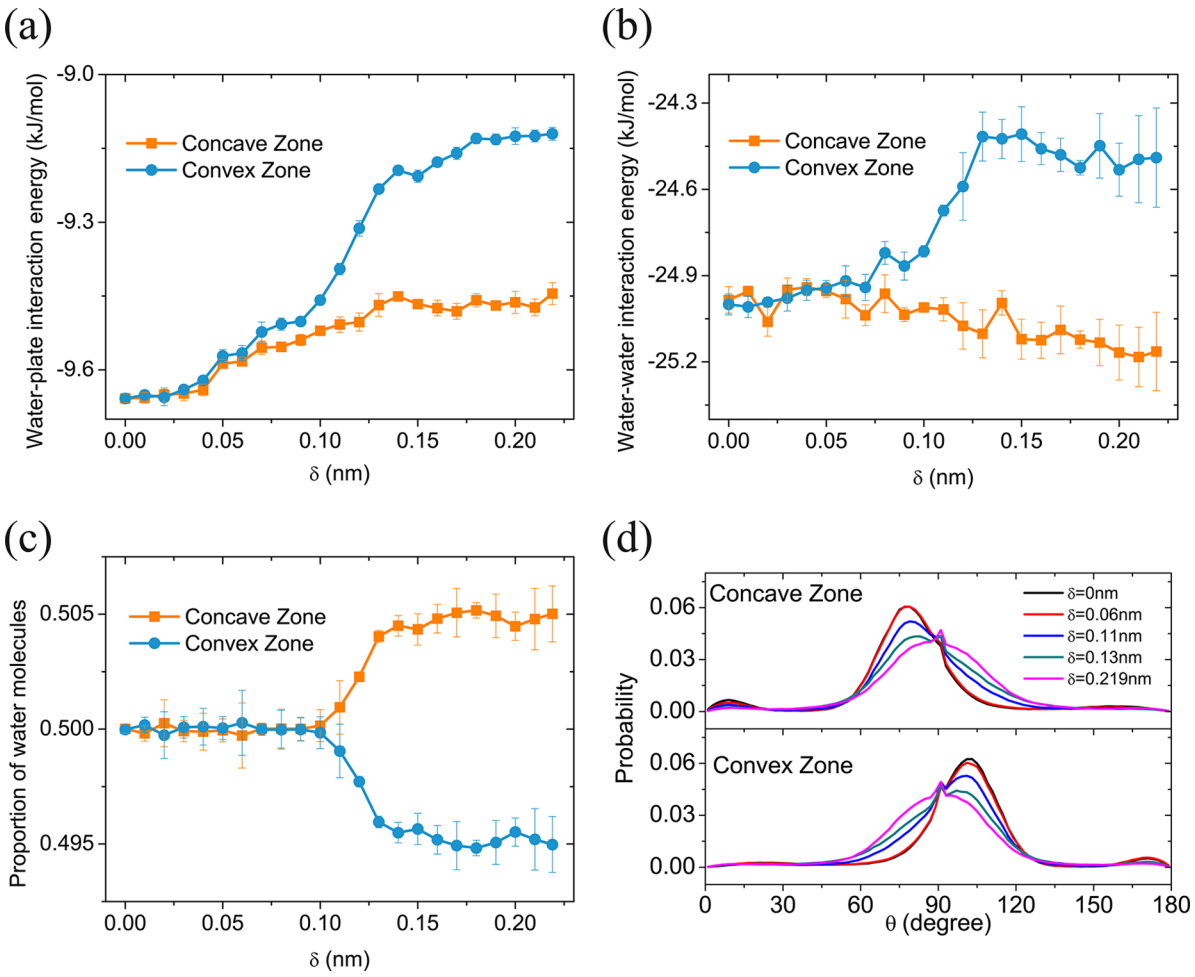

Figure 4. (a) Average water−plate interaction energies in the concave and convex zones (described in Figure 1d−f) with respect to δ. The interaction energies in both zones increase with increasing δ, whereas their difference starts to increase extensively when δ = 0.11 nm. (b) The average water−water interaction energy for the concave or convex zone as a function of δ. (c) The proportions of numbers of water molecules located in the concave and convex zones. The numbers of water molecules in two zones are almost equal until $\delta \geq 0.11$ nm. (d) The probability distribution of angles between the Z axis and water molecular dipoles within the two types of zones in systems with δ = 0, 0.06, 0.11, 0.13, and 0.219 nm. As δ increases, the water dipoles in both zones tend to be parallel to the plates.

attraction or stronger repulsion between water molecules. Thus, the weaker water−plate attraction and the stronger water−water repulsion in the convex zone lead to a higher potential barrier for water; on the contrary, it is easier for water molecules to diffuse into the concave zone. We calculate the proportion of number of water molecules located in the concave and convex zones with respect to δ, respectively, as shown in Figure 4c. When δ ranges from 0 to 0.1 nm, the numbers of water molecules in the two zones are almost equal, as evidenced by the values of their proportion, 0.5. Such a uniform distribution of water molecules corresponds to the ice structure. When $\delta \geq 0.11$ nm, the equality breaks down. The number of water molecules in the concave zone enhances sharply when 0.1 nm $\leq \delta \leq$ 0.13 nm, whereas it decreases in the convex zone. This indicates that the difference between the local confinements in the two zones is large enough for the uneven distribution of water molecules. When $\delta \geq 0.13$ nm, their difference fluctuates within a small range. Such an uneven distribution of water molecules is also an indication of the breaking down of ice networks. This phenomenon corresponds well to the result in Figure 2a.

Water molecular orientation is also studied. Figure 4d presents the probability distribution of angles between water molecular dipole moments and the Z axis in concave and convex zones. For one water molecule, water dipole is defined as the vector sum of two H−M atoms (here, M denotes the dummy atom, which carries negative charge). And the angle between the water dipole and Z axis is also averaged over the molecules and trajectories. With increasing δ, water molecular dipoles in both zones tend to be parallel to the plates. This can be understood from Figure 3a. As δ increases, water is squeezed by the stronger confinement. Also, because the two plates are more symmetric, interactions between water and plates are more symmetric too. Besides the strengthening and more symmetric confinement of the plates, the unequal amount of water molecules in the two types of zones may also lead to the parallel preference. When the distribution of water molecules is even, the molecules exist in the form of a puckered structure, and the attraction between water molecules in different oxygen planes (also in different zones) makes water molecules not parallel to the plates. However, as δ increases, the confinement becomes stronger and more symmetric, which makes water molecules parallel to the plates, and the unequal distribution of water molecules weakens the attraction between water molecules in different zones, causing water molecules to be parallel to the plates. Note that the occurrence of the sharpened

DOI: 10.1021/acs.jpcb.6b02473
J. Phys. Chem. B 2016, 120, 9011−9018

peak at 90° implies the remarkable concentrated distribution of water molecules whose dipoles are parallel to the plates. Such a distribution originates from the extremely strong confinement of our systems (d = 0.79 nm, which only accommodates one layer of water molecules).

4.3. Hydrogen Bonding. A manifestation for the transition of states of water is the variation of hydrogen bonding. We check this by calculating the average number of hydrogen bonds (H-bonds) formed by one water molecule with its neighboring water molecules in the same oxygen plane, N_{intra}, and with the water molecules in another oxygen plane, N_{inter}, as plotted in Figure 5a. According to Figure 3b, it is obvious that

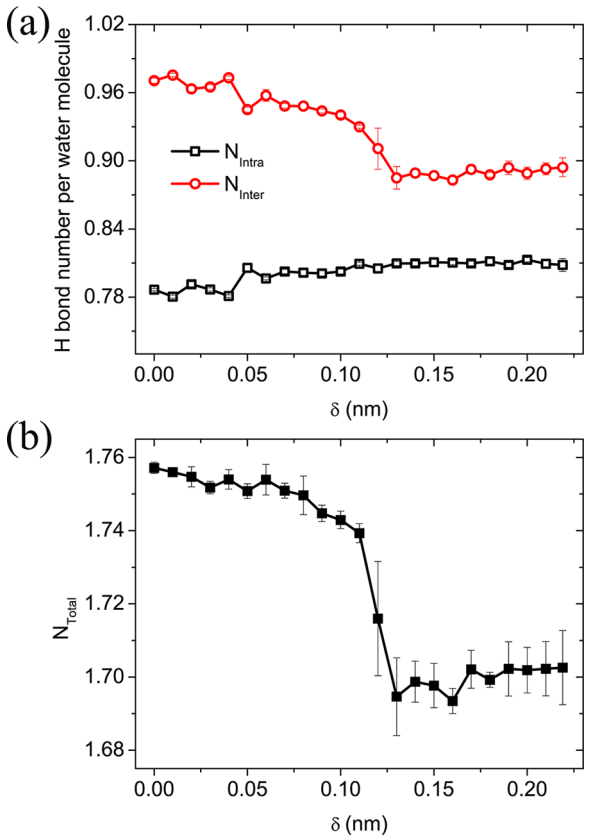

Figure 5. (a) Profile of average number of H-bonds formed by one water molecule with neighboring water molecules within the same oxygen plane, N_{intra}, and in another oxygen plane, N_{inter}, with respect to δ. (b) The sum (N_{total}) of N_{intra} and N_{inter}. N_{inter} exhibits a similar tendency to N_{total}, and both of them start decreasing sharply at δ = 0.11 nm. N_{intra} increases gradually before δ = 0.11 nm and then remains nearly unchanged.

two water sublayers appear (as measured by the O positions) and are symmetric with respect to the middle plane of the system. Then, oxygen planes can be separated by the middle plane. N_{intra} increases gradually before δ = 0.11 nm and then remains nearly unchanged. N_{inter} decreases gradually first and drops sharply when δ ranges from 0.11 to 0.13 nm. Figure 5b shows the sum of N_{intra} and N_{inter}, N_{total}, with respect to δ. H-bonds present a constraint between water molecules, so the reduction in the number of H-bonds indicates the disruption of ice networks and increases water mobility. Thus, the tendency of N_{total} corresponds well to the results in Figure 2a. Obviously, N_{total} has a similar evolution to that of N_{inter}, indicating that N_{inter} plays a predominant role in the variation of hydrogen bonding. Because the numbers of water molecules in the concave and convex zones are unequal, the original puckered ice structure is disrupted. Thus, the H-bonds between two oxygen planes are broken, and N_{inter} diminishes, indicating that the melting process occurs.

5. CONCLUSIONS

In summary, on the basis of MD simulations, we have treated phosphorene as a model material to show the water melting−freezing transitions induced by the mismatch of confining plates with nonflat surfaces. As δ varies from 0 nm to 0.5α, a melting process is observed at 230 K, and an inverse process occurs when δ increases from 0.5α to α. Upon increasing the degree of mismatch between the plates (δ = 0 nm to 0.5α), water is squeezed by the strengthening degree of global confinement. Furthermore, the disparate variations of local confinements in the concave and convex zones lead to the uneven distribution of water molecules, which disrupts the network of water molecules.

This work explores that the water dynamics can also be greatly affected by the nonflat surface of plates with confinement, which suggests a new melting mechanism for water at an even lower temperature than that in previous works[25,27] and provides a guidance for acquiring liquid water at a temperature below the freezing point. The phenomena reported herein might enrich the knowledge on water and inspire more applications of similar materials.

AUTHOR INFORMATION

Corresponding Authors

*E-mail: jyhuang@fudan.edu.cn (J.Y.H.).
*E-mail: jphuang@fudan.edu.cn. Tel: +86-21-55665227 (J.P.H.).

Notes

The authors declare no competing financial interest.

ACKNOWLEDGMENTS

We thank Yu Wang, Ruxi Qi, Tong Qiu, and Likai Li for their fruitful help and discussion. We acknowledge the financial support by the Science and Technology Commission of Shanghai Municipality under Grant No. 16ZR1445100.

REFERENCES

(1) de Groot, B. L.; Grubmuller, H. Water permeation across biological membranes: Mechanism and dynamics of aquaporin-1 and GlpF. *Science* **2001**, *294*, 2353−2357.
(2) Stepniewski, M.; Bunker, A.; Pasenkiewicz-Gierula, M.; Karttunen, M.; Rog, T. Effects of the lipid bilayer phase state on the water membrane interface. *J. Phys. Chem. B* **2010**, *114*, 11784−11792.
(3) Fumagalli, M.; Lyonnard, S.; Prajapati, G.; Berrod, Q.; Porcar, L.; Guillermo, A.; Gebel, G. Fast water diffusion and long-term polymer reorganization during nafion membrane hydration evidenced by time-resolved small-angle neutron scattering. *J. Phys. Chem. B* **2015**, *119*, 7068−7076.
(4) Gong, X. J.; Li, J. Y.; Zhang, H.; Wan, R. Z.; Lu, H. J.; Wang, S.; Fang, H. P. Enhancement of water permeation across a nanochannel by the structure outside the channel. *Phys. Rev. Lett.* **2008**, *101*, No. 257801.
(5) Wang, Y.; Zhao, Y. J.; Huang, J. P. Giant pumping of single-file water molecules in a carbon nanotube. *J. Phys. Chem. B* **2011**, *115*, 13275−13279.
(6) Meng, X. W.; Wang, Y.; Zhao, Y. J.; Huang, J. P. Gating of a water nanochannel driven by dipolar molecules. *J. Phys. Chem. B* **2011**, *115*, 4768−4773.

DOI: 10.1021/acs.jpcb.6b02473
J. Phys. Chem. B 2016, 120, 9011−9018

(7) Qiu, T.; Meng, X. W.; Huang, J. P. Nonstraight nanochannels transfer water faster than straight nanochannels. *J. Phys. Chem. B* **2015**, *119*, 1496−1502.
(8) Service, R. F. Desalination freshens up. *Science* **2006**, *313*, 1088−1090.
(9) Akin, I.; Zor, E.; Bingol, H.; Ersoz, M. Green synthesis of reduced graphene oxide/polyaniline composite and its application for salt rejection by polysulfone-based composite membranes. *J. Phys. Chem. B* **2014**, *118*, 5707−5716.
(10) Corry, B. Designing carbon nanotube membranes for efficient water desalination. *J. Phys. Chem. B* **2008**, *112*, 1427−1434.
(11) Bhushan, B.; Israelachvili, J. N.; Landman, U. Nanotribology: Friction, wear and lubrication at the atomic scale. *Nature* **1995**, *374*, 607−616.
(12) Zhu, Y. X.; Granick, S. Viscosity of interfacial water. *Phys. Rev. Lett.* **2001**, *87*, No. 096104.
(13) Zhou, R. H.; Huang, X. H.; Margulis, C. J.; Berne, B. J. Hydrophobic collapse in multidomain protein folding. *Science* **2004**, *305*, 1605−1609.
(14) Liu, P.; Huang, X. H.; Zhou, R. H.; Berne, B. J. Observation of a dewetting transition in the collapse of the melittin tetramer. *Nature* **2005**, *437*, 159−162.
(15) Berne, B. J.; Weeks, J. D.; Zhou, R. H. Dewetting and hydrophobic interaction in physical and biological systems. *Annu. Rev. Phys. Chem.* **2009**, *60*, 85−103.
(16) Markiewicz, B. N.; Mukherjee, D.; Troxler, T.; Gai, F. Utility of 5-cyanotryptophan fluorescence as a sensitive probe of protein hydration. *J. Phys. Chem. B* **2016**, *120*, 936−944.
(17) Kumar, P.; Buldyrev, S. V.; Starr, F. W.; Giovambattista, N.; Stanley, H. E. Thermodynamics, structure, and dynamics of water confined between hydrophobic plates. *Phys. Rev. E* **2005**, *72*, No. 051503.
(18) Giovambattista, N.; Rossky, P. J.; Debenedetti, P. G. Computational studies of pressure, temperature, and surface effects on the structure and thermodynamics of confined water. *Annu. Rev. Phys. Chem.* **2012**, *63*, 179−200.
(19) Zangi, R.; Mark, A. E. Monolayer ice. *Phys. Rev. Lett.* **2003**, *91*, No. 025502.
(20) Giovambattista, N.; Rossky, P. J.; Debenedetti, P. G. Phase transitions induced by nanoconfinement in liquid water. *Phys. Rev. Lett.* **2009**, *102*, 050603.
(21) Giovambattista, N.; Rossky, P. J.; Debenedetti, P. G. Effect of pressure on the phase behavior and structure of water confined between nanoscale hydrophobic and hydrophilic plates. *Phys. Rev. E* **2006**, *73*, 041604.
(22) Giovambattista, N.; Rossky, P. J.; Debenedetti, P. G. Effect of temperature on the structure and phase behavior of water confined by hydrophobic, hydrophilic, and heterogeneous surfaces. *J. Phys. Chem. B* **2009**, *113*, 13723−13734.
(23) Zangi, R.; Mark, A. E. Electrofreezing of confined water. *J. Chem. Phys.* **2004**, *120*, 7123.
(24) Hu, X.; Elghobashi-Meinhardt, N.; Gembris, D.; Smith, J. C. Response of water to electric fields at temperatures below the glass transition: A molecular dynamics analysis. *J. Chem. Phys.* **2011**, *135*, No. 134507.
(25) Qiu, H.; Guo, W. L. Electromelting of confined monolayer ice. *Phys. Rev. Lett.* **2013**, *110*, No. 195701.
(26) Qian, Z. Y.; Wei, G. H. Electric-field-induced phase transition of confined water nanofilms between two graphene sheets. *J. Phys. Chem. A* **2014**, *118*, 8922−8928.
(27) Mei, F.; Zhou, X. Y.; Kou, J. L.; Wu, F. M.; Wang, C. L.; Lu, H. J. A transition between bistable ice when coupling electric field and nanoconfinement. *J. Chem. Phys.* **2015**, *142*, No. 134704.
(28) Koga, K.; Tanaka, H. Phase diagram of water between hydrophobic surfaces. *J. Chem. Phys.* **2005**, *122*, No. 104711.
(29) Li, Q.; Song, J.; Besenbacher, F.; Dong, M. D. Two-dimensional material confined water. *Acc. Chem. Res.* **2015**, *48*, 119−127.
(30) Eng, P. J.; Trainor, T. P.; Brown, G. E.; Waychunas, G. A.; Newville, M.; Sutton, S. R.; Rivers, M. L. Structure of the hydrated alpha-Al_2O_3 (0001) surface. *Science* **2000**, *288*, 1029−1033.
(31) Aarts, I. M. P.; Pipino, A. C. R.; Hoefnagels, J. P. M.; Kessels, W. M. M.; van de Sanden, M. C. M. Quasi-ice monolayer on atomically smooth amorphous SiO_2 at room temperature observed with a high-finesse optical resonator. *Phys. Rev. Lett.* **2005**, *95*, No. 166104.
(32) Li, L.; Yu, Y.; Ye, G. J.; Ge, Q.; Ou, X.; Wu, H.; Feng, D.; Chen, X. H.; Zhang, Y. Black phosphorus field-effect transistors. *Nat. Nanotechnol.* **2014**, *9*, 372−377.
(33) Liu, H.; Neal, A. T.; Zhu, Z.; Luo, Z.; Xu, X. F.; Tomanek, D.; Ye, P. D. Phosphorene: An unexplored 2D semiconductor with a high hole mobility. *ACS Nano* **2014**, *8*, 4033−4041.
(34) Lu, W. L.; Nan, H. Y.; Hong, J. H.; Chen, Y. M.; Zhu, C.; Liang, Z.; Ma, X. Y.; Ni, Z. H.; Jin, C. H.; Zhang, Z. Plasma-assisted fabrication of monolayer phosphorene and its Raman characterization. *Nano Res.* **2014**, *7*, 853−859.
(35) Service, R. F. Beyond graphene. *Science* **2015**, *348*, 490−492.
(36) Xia, F.; Wang, H.; Jia, Y. Rediscovering black phosphorus as an anisotropic layered material for optoelectronics and electronics. *Nat. Commun.* **2014**, *5*, No. 4458.
(37) Chen, L.; Zhou, G. M.; Liu, Z. B.; Ma, X. M.; Chen, J.; Zhang, Z. Y.; Ma, X. L.; Li, F.; Cheng, H. M.; Ren, W. C. Scalable clean exfoliation of high-quality few-layer black phosphorus for a flexible lithium ion battery. *Adv. Mater.* **2016**, *28*, 510.
(38) Mao, N. N.; Tang, J. Y.; Xie, L. M.; Wu, J. X.; Han, B. W.; Lin, J. J.; Deng, S. B.; Ji, W.; Xu, H.; Liu, K. H.; Tong, L. M.; Zhang, J. Optical anisotropy of black phosphorus in the visible regime. *J. Am. Chem. Soc.* **2016**, *138*, 300−305.
(39) Pei, J. J.; Gai, X.; Yang, J.; Wang, X. B.; Yu, Z. F.; Choi, D. Y.; Luther-Davies, B.; Lu, Y. R. Producing air-stable monolayers of phosphorene and their defect engineering. *Nat. Commun.* **2016**, *7*, No. 10450.
(40) Allain, A.; Kang, J. H.; Banerjee, K.; Kis, A. Electrical contacts to two-dimensional semiconductors. *Nat. Mater.* **2015**, *14*, 1195−1205.
(41) Luo, Z.; Maassen, J.; Deng, Y. X.; Du, Y. C.; Garrelts, R. P.; Lundstrom, M. S.; Ye, P. D.; Xu, X. F. Anisotropic in-plane thermal conductivity observed in few-layer black phosphorus. *Nat. Commun.* **2015**, *6*, No. 8572.
(42) Favron, A.; Gaufres, E.; Fossard, F.; Phaneuf-L'Heureux, A. L.; Tang, N. Y. W.; Levesque, P. L.; Loiseau, A.; Leonelli, R.; Francoeur, S.; Martel, R. Photooxidation and quantum confinement effects in exfoliated black phosphorus. *Nat. Mater.* **2015**, *14*, 826.
(43) Buscema, M.; Groenendijk, D. J.; Blanter, S. I.; Steele, G. A.; van der Zant, H. S. J.; Castellanos-Gomez, A. Fast and broadband photoresponse of few-layer black phosphorus field-effect transistors. *Nano Lett.* **2014**, *14*, 3347−3352.
(44) Buscema, M.; Groenendijk, D. J.; Steele, G. A.; van der Zant, H. S. J.; Castellanos-Gomez, A. Photovoltaic effect in few-layer black phosphorus PN junctions defined by local electrostatic gating. *Nat. Commun.* **2014**, *5*, No. 4651.
(45) Sresht, V.; Padua, A. A. H.; Blankschtein, D. Liquid-phase exfoliation of phosphorene: Design rules from molecular dynamics simulations. *ACS Nano* **2015**, *9*, 8255−8268.
(46) Wang, Z. H.; Jia, H.; Zheng, X. Q.; Yang, R.; Wang, Z. F.; Ye, G. J.; Chen, X. H.; Shan, J.; Feng, P. X. L. Black phosphorus nanoelectromechanical resonators vibrating at very high frequencies. *Nanoscale* **2015**, *7*, 877−884.
(47) Zhang, W.; Ye, C.; Bi, B.; Yang, Z. X.; Zhou, R. H. Wetting and Diffusion of Water on Pristine and Strained Phosphorene. http://arxiv.org/abs/1512.02116.
(48) Jorgensen, W. L.; Chandrasekhar, J.; Madura, J. D.; Impey, R. W.; Klein, M. L. Comparison of simple potential functions for simulating liquid water. *J. Chem. Phys.* **1983**, *79*, 926.
(49) Koga, K.; Zeng, X. C.; Tanaka, H. Freezing of confined water: A bilayer ice phase in hydrophobic nanopores. *Phys. Rev. Lett.* **1997**, *79*, 5262.

DOI: 10.1021/acs.jpcb.6b02473
J. Phys. Chem. B 2016, 120, 9011−9018

(50) Koga, K.; Gao, G. T.; Tanaka, H.; Zeng, X. C. Formation of ordered ice nanotubes inside carbon nanotubes. *Nature* **2001**, *412*, 802−805.
(51) Hess, B.; Kutzner, C.; van der Spoel, D.; Lindahl, E. GROMACS 4: Algorithms for highly efficient, load-balanced, and scalable molecular simulation. *J. Chem. Theory Comput.* **2008**, *4*, 435.
(52) Darden, T. A.; York, D. M.; Pedersen, L. G. Particle mesh Ewald: An N·log(N) method for Ewald sums in large systems. *J. Chem. Phys.* **1993**, *98*, 10089.
(53) Nosé, S. A unified formulation of the constant temperature molecular dynamics methods. *J. Chem. Phys.* **1984**, *81*, 511.
(54) Hoover, W. G. Canonical dynamics: Equilibrium phase-space distributions. *Phys. Rev. A* **1985**, *31*, 1695.
(55) Yeh, I.-C.; Berkowitz, M. L. Ewald summation for systems with slab geometry. *J. Chem. Phys.* **1999**, *111*, 3155.

DOI: 10.1021/acs.jpcb.6b02473
J. Phys. Chem. B 2016, 120, 9011−9018